JOURNAL OF THERMOPHYSICS AND HEAT TRANSFER
Vol. 23, No. 4, October–December 2009

Two Methods for Solving Radiative Transfer in a Two-Dimensional Graded-Index Medium

Yong Huang,* Kai Wang, and Jun Wang
Beijing University of Aeronautics and Astronautics, 100191 Beijing, People's Republic of China

DOI: 10.2514/1.41819

Two methods are presented for the study of radiative heat transfer in a two-dimensional graded-index semitransparent medium. One is a combination of the cell model and the ray-tracing technique, and the other is a combination of the linear refractive-index cell model and the discrete curved-ray-tracing technique. The medium is discretized into many cells. The constant-refractive-index assumption is used in the first model and the linear approximation of refractive index is used in the second model. We have compared the results and the calculation efficiency of these two methods, as well as the heat transfer at radiative equilibrium. The results of the two methods show little difference. We also studied the radiative heat transfer properties of the medium, and the results show that the refractive-index distribution has great influence on the temperature field. That is, the medium with various types of graded index has a higher or lower temperature than the medium with a constant refractive index. The medium also has a flat temperature field or a sharper temperature field than the constant-refractive-index medium. This is due to internal total reflection in the graded-index medium.

Nomenclature

a_{im}	=	coefficient denoting the influence of node m to node i
b	=	index of a boundary segment, $1–(2N_x + 2N_y)$
c_{ik}	=	coefficient denoting the influence of boundary node k to node i
I	=	radiative intensity, $\mathrm{W/m^2 \cdot sr}$
i	=	index of a cell in the x direction
j	=	index of a cell in the y direction
L	=	side length of the medium, m
m	=	index of a cell of the medium, $1–N_xN_y$
mi	=	ith cell of the medium through which the ray passes ($i = 1–p$ and p varies for each ray)
N	=	number of nodes
$n_{i,j}$	=	refractive index in a cell
p	=	number of the cell through which the ray passes
q	=	qth segment of the boundary that is at the end of the ray-tracing
s	=	distance along the ray trajectory, m
s_i	=	distance a ray travels when passing through the ith cell ($i = 1 \sim p$ and p varies for each ray), m
T	=	temperature, K
$T_{\max}$	=	maximum value of the temperature in the medium, K
$T_{\min}$	=	minimum value of the temperature in the medium, K
T_{standard}	=	temperature calculated by the curved-ray-tracing method in a 40×40 spatial mesh and a 70×70 directional mesh, K
x, y	=	Cartesian coordinates, m
δ	=	relative error of the calculated temperature from T_{standard} or benchmark solution
$\Delta x, \Delta y$	=	length of a cell in the x direction and y direction, m
ΔT	=	temperature difference from T_{standard}, K
θ	=	polar angle, deg
θ_i	=	discrete polar angle ($i = 1–N_\theta$), deg
κ	=	absorption coefficient, $\mathrm{m^{-1}}$
σ	=	Stefan–Boltzmann constant, 5.67×10^{-8} $\mathrm{W/(m^2 \cdot K^4)}$
φ	=	azimuthal angle, deg
φ_j	=	discrete azimuthal angle ($j = 1–N_\varphi$), deg
Ω	=	local direction vector

Subscripts

b	=	black body
bi	=	segment of boundary, $i = 1–(2N_x + 2N_y)$
bq	=	qth segment of the boundary which is at the end of the ray-tracing
m	=	medium
mi	=	ith cell of the medium which the ray passes through ($i = 1–p$ and p varies for each ray)
x, y	=	x and y directions
θ	=	polar angle
φ	=	azimuthal angle

I. Introduction

RADIATIVE heat transfer in a graded-index (GRIN) medium can be found in many processes, such as the heating of glass and thermal protective coatings, manufacturing of waveguide materials, and ray propagation through the atmosphere, as well as the optical measurement in flames and other semitransparent media. The rays propagating inside a GRIN medium are not straight lines, but curved lines, which are governed by minimization of the Fermat principle [1]. Based on this principle, total reflection will occur within the medium. The refractive index has significant influence on the radiative transfer in the medium.

Recently, some researchers have turned their efforts toward radiative transfer in a GRIN medium. In 2000, Ben Abdallah and Le Dez [2] put forward a curved-ray-tracing technique to solve for the radiation transfer in a GRIN medium and first analyzed the thermal emission of a semitransparent slab with a variable spatial refractive index. By this method, they also investigated radiation heat transfer and coupled radiation–conduction inside a semitransparent slab with a variable spatial refractive index [3,4] as well as the thermal emission of a two-dimensional rectangular cavity [5]. In 2001, Huang et al. [6] proposed a combination of a pseudo-source-adding method and a ray-splitting/tracing method to study the apparent thermal emission of a semitransparent slab with a graded index and gray diffuse substrate. They also studied the temperature field of a

Received 27 October 2008; revision received 28 April 2009; accepted for publication 30 April 2009.

*School of Aeronautical Science and Engineering, 37 Xueyuan Road, Haidian District, Mailbox 505; huangy_zl@263.net (Corresponding Author).

slab with a linear refractive-index distribution and gray walls [7]. Lemonnier and Le Dez [8] presented a discrete ordinates solution for radiative transfer across a slab with variable refractive index. Yi et al. [9] and Tan et al. [10] studied transient radiative heat transfer in a GRIN semitransparent slab. Recently, some other methods have been investigated by many researchers, such as the discrete curved-ray-tracing method [11], the finite volume method [12], the meshless method [13], the discrete transfer method [14], the Chebyshev collocation spectral method [15], the finite element method [16], the least-squares finite element method [17], the discontinuous finite element method [18], and the least-squares spectral element method [19].

Most researchers who have investigated this topic have discussed one-dimensional problems, and some have explored multidimensional problems [11,12,16–19]. In the early 1990s, Siegel and Spuckler [20] developed a model for a one-dimensional composite medium with several sublayers. Each sublayer was treated as a slab with a uniform index bounded by diffuse surfaces. The authors expressed the idea that increasing the number of sublayers could approach the radiative behavior of a medium with a continuously varying refractive index. We have proven that Siegel and Spuckler's idea can be employed to solve multidimensional problems, and a cell model was presented for solution of the apparent emission from two-dimensional semitransparent GRIN media [21]. Recently, a linear refractive-index (LRI) cell model was presented for the solution of radiative transfer in a two-dimensional GRIN medium. Using the LRI cell model gives more precise numerical results than those of the cell model [22].

Because little is known about the radiative heat transfer properties of a multidimensional GRIN medium, this paper will study the temperature fields of radiative equilibrium in a two-dimensional GRIN medium. Two methods are presented for calculation. One method is the combination of the cell model and the ray-tracing technique (cell-RT), and the other is the combination of the LRI cell model and the discrete curved-ray-tracing technique (LRIC-CRT). We will compare these two methods and then study the temperature fields of the media.

II. Physical Model and Solution Methods

A. Physical Model

In this paper, we study the temperature field $T(x, y)$ of a two-dimensional medium (see Fig. 1). The medium has a cross-sectional area of $L_x \times L_y$ (m^2) and is assumed to be a nonscattering gray medium with absorption coefficient κ and refractive-index distribution $n(x, y)$. The four boundaries of the medium are black with temperatures T_1, T_2, T_3, and T_4. The medium is at radiative equilibrium.

B. Two Approximate Models

Rays propagating inside a GRIN medium are not straight lines, but are curved lines, which are governed by minimization of the Fermat principle [1]. A difficulty in the study of thermal radiative transfer in a GRIN medium is that the solution of the ray trajectories is very complex, especially when the medium has multidimensional refractive-index distributions.

In our previous papers [21,22], we have presented two approximate models: the cell model and the LRI cell model, respectively. The medium is discretized into many cells in these models (see Fig. 2). The cell model includes two hypotheses [21]:

1) The refractive-index distribution of the medium $n(x, y)$ is changed to a discrete form:

$$n_{i,j} = n[(i-0.5)\Delta x, (j-0.5)\Delta y] \quad (i = 1, 2, \ldots, N_x; j = 1, 2, \ldots, N_y) \tag{1}$$

where N_x and N_y are the numbers of cells of the medium in the x direction and y direction, respectively, and $\Delta x = L_x/N_x$ and $\Delta y = L_y/N_y$ are the lengths of the cells in the x direction and y direction, respectively. Based on this change, every cell has its own unique refractive index, and a ray propagates in a straight path within every cell.

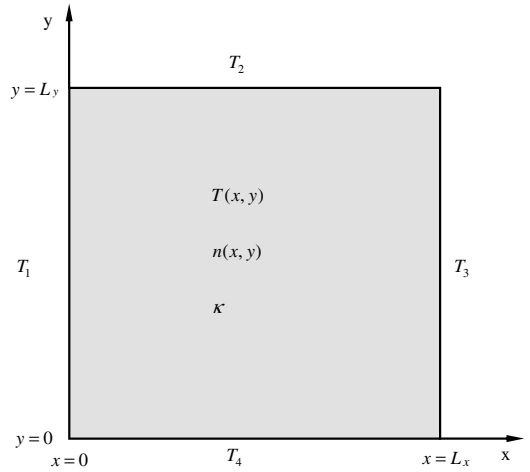

Fig. 1 Physical model of a two-dimensional GRIN medium.

2) The interface between two cells is assumed to be a refraction/total reflection interface. This means that we only consider total reflection at the interface. If we adopt a refraction/reflection interface model, it will introduce large errors into the results.

The linear refractive-index cell model includes the following three hypotheses [22]:

1) The refractive-index distribution of the medium $n(x, y)$ is changed to a discrete form:

$$\begin{aligned} n_{i,j}(x) &= n[(i-1)\Delta x, (j-0.5)\Delta y] \\ &\quad + \frac{x-(i-1)\Delta x}{\Delta x}\{n[i\Delta x, (j-0.5)\Delta y] \\ &\quad - n[(i-1)\Delta x, (j-0.5)\Delta y]\} \\ &\quad (i = 1, 2, \cdots, N_x; j = 1, 2, \cdots, N_y) \end{aligned} \tag{2}$$

Based on this hypothesis, every cell has a one-dimensional linear refractive-index distribution. Some papers have discussed how to calculate the curved trajectories in a one-dimensional linear refractive-index medium [2–4,7,21,22].

2) The interface between two cells is assumed to be a refraction/total reflection interface.

3) In each cell, all rays propagate in a two-dimensional plane. In the two-dimensional medium shown in Fig. 1, only the rays parallel to the XOY plane have a two-dimensional trajectory, and others will have a three-dimensional trajectory. To simplify the calculations, we

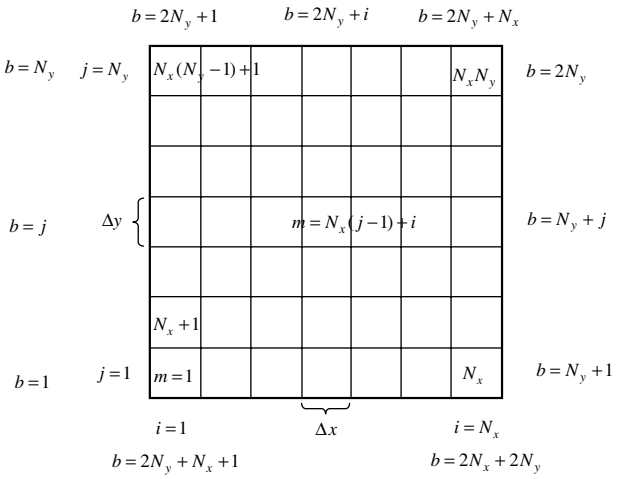

Fig. 2 Discretization of medium and boundaries. The index of the spatial nodes ranges from $m = 1$ to $m = N_x \times N_y$; the index of the boundary segments ranges from $b = 1$ to $2N_x + 2N_y$.

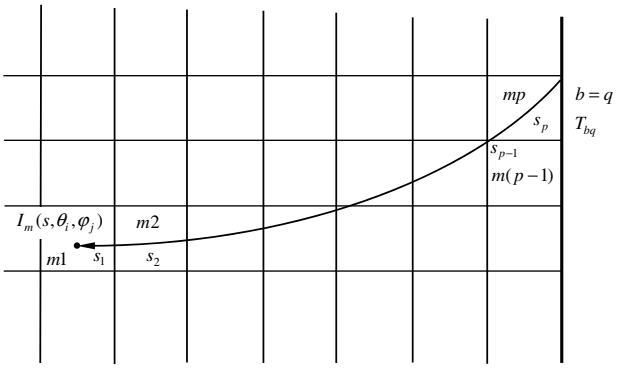

Fig. 3 Tracing back the path of $I_m(s, \theta_i, \varphi_j)$ to the boundary, the ray passes through *mp* cells.

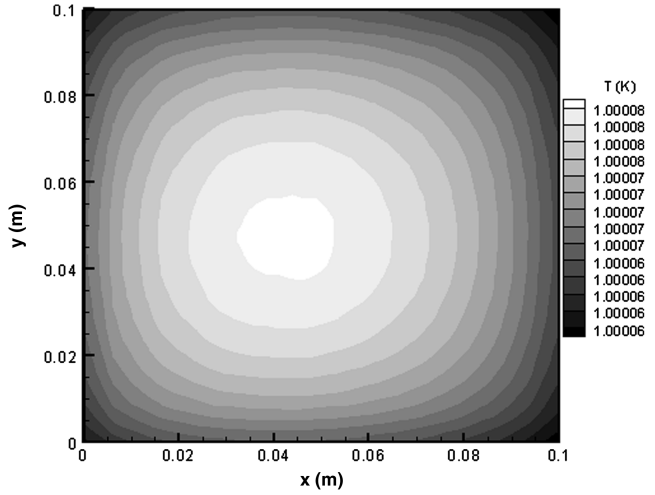

Fig. 4 Temperature map of a medium using LRIC-CRT for 1 K boundary temperatures; $n(x,y) = 1.1 + 0.6x/L_x + 0.2y/L_y$, $\kappa = 10\ \mathrm{m}^{-1}$, $L_x = L_y = 0.1$ m, $N_x = N_y = 40$, and $N_\theta = N_\varphi = 50$.

present this third hypothesis. The numerical results show that this hypothesis is reasonable [22].

For the LRI cell model using a higher-precision approach to the real refractive-index distribution, the results show that this approximate model can bring higher precision to the radiative transfer calculation [22].

C. Solution to the Radiative Equilibrium Temperature Field in a Medium

The governing equation for radiative transfer in a GRIN medium is

$$\frac{\mathrm{d}}{\mathrm{d}s}\left[\frac{I(s,\Omega)}{n^2(s)}\right] + \kappa\frac{I(s,\Omega)}{n^2(s)} = \kappa I_b(s) \tag{3}$$

where $I_b(s)$ is the Planck function for the temperature at position s, and Ω is the local direction vector.

For radiative equilibrium, the heat transfer in the medium is only by radiation, and the radiative energy isotropically emitted from any point within the medium equals that directionally absorbed over the whole space. Thus, the energy-balance equation is

$$\begin{aligned} 4n^2(s)\sigma T^4(s) &= \int_{\Omega=4\pi} I_m(s,\Omega)\mathrm{d}\Omega \\ &= \int_0^{2\pi}\int_0^{\pi} I_m(s,\theta,\varphi)\sin\theta\mathrm{d}\theta\mathrm{d}\varphi \end{aligned} \tag{4}$$

where $I_m(s, \Omega)$ is the radiative intensity of the medium at position s and in the direction Ω, θ is the polar angle, and φ is the azimuthal angle. We divide the spatial direction into N_θ discrete polar angles and N_φ discrete azimuthal angles. Hence, the right side of Eq. (4) can be written as in discrete form as

$$\int_0^{2\pi}\int_0^{\pi} I_m(s,\theta,\varphi)\sin\theta\mathrm{d}\theta\mathrm{d}\varphi = \sum_{j=1}^{N_\varphi}\sum_{i=1}^{N_\theta} I_m(s,\theta_i,\varphi_j)\sin\theta_i\frac{\pi}{N_\theta}\frac{2\pi}{N_\varphi} \tag{5}$$

Because the medium has been discretized into $N_x \times N_y$ cells (see Fig. 2) and the boundaries have been discretized into $2N_x + 2N_y$ segments, the temperature of each segment of the boundary is

$$\begin{cases} T_{bi} = T_1 & i = 1 \sim N_y \\ T_{bi} = T_3 & i = (N_y + 1) \sim 2N_y \\ T_{bi} = T_2 & i = (2N_y + 1) \sim (2N_y + N_x) \\ T_{bi} = T_4 & i = (2N_y + N_x + 1) \sim (2N_y + 2N_x) \end{cases} \tag{6}$$

We assume that each cell has a uniform temperature T_i (i= $1, 2, \ldots, N_x \times N_y$). By solving Eq. (3), we get (see Fig. 3)

Table 1 Comparison with the results of Monte Carlo benchmark solution for two node sets[a]

		$N_x = N_y = 20$		$N_x = N_y = 20$		$N_x = N_y = 60$		$N_x = N_y = 60$	
y/L_y	Benchmark solution [23] T/T_4	Cell-RT	δ%	LRIC-CRT	δ%	Cell-RT	δ%	LRIC-CRT	δ%
0.025	0.883	0.883	0	0.883	0	0.884	0.11	0.884	0.11
0.075	0.863	0.863	0	0.863	0	0.865	0.23	0.864	0.11
0.125	0.845	0.844	0.12	0.844	0.12	0.846	0.12	0.845	0
0.175	0.828	0.828	0	0.828	0	0.829	0.12	0.828	0
0.225	0.812	0.812	0	0.812	0	0.813	0.12	0.812	0
0.275	0.797	0.797	0	0.797	0	0.798	0.13	0.798	0.13
0.325	0.783	0.783	0	0.783	0	0.784	0.13	0.784	0.13
0.375	0.77	0.769	0.13	0.77	0	0.771	0.13	0.771	0.13
0.425	0.758	0.756	0.26	0.756	0.26	0.758	0	0.758	0
0.475	0.746	0.745	0.13	0.746	0	0.747	0.13	0.746	0
0.525	0.736	0.734	0.27	0.736	0	0.737	0.14	0.736	0
0.575	0.726	0.724	0.28	0.725	0.14	0.728	0.28	0.727	0.14
0.625	0.716	0.713	0.42	0.714	0.28	0.717	0.14	0.716	0
0.675	0.707	0.705	0.28	0.706	0.14	0.708	0.14	0.707	0
0.725	0.698	0.693	0.72	0.695	0.43	0.698	0	0.698	0
0.775	0.69	0.687	0.43	0.688	0.29	0.69	0	0.689	0.14
0.825	0.681	0.677	0.59	0.679	0.29	0.679	0.29	0.679	0.29
0.875	0.671	0.667	0.6	0.668	0.45	0.67	0.15	0.67	0.15
0.925	0.661	0.651	1.51	0.652	1.36	0.656	0.76	0.656	0.76
0.975	0.643	0.627	2.49	0.628	2.33	0.643	0	0.642	0.16

[a] $n(x, y) = 5[1 - 0.4356(x^2/L_x^2 + y^2/L_y^2)]^{0.5}$, $T_1 = T_2 = T_3 = 0$ K, $T_4 = 1000$ K, $\kappa = 10\ \mathrm{m}^{-1}$, $L_x = L_y = 0.1$ m, $x/L_x = 0.325$, and $N_\theta = N_\varphi = 50$.

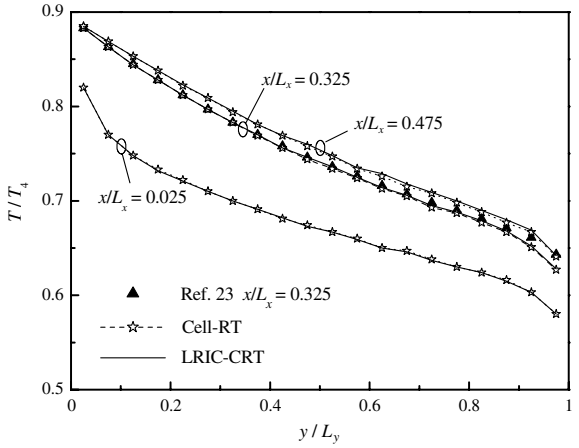

Fig. 5 Comparison of the results from LRIC-CRT, cell-RT, and Monte Carlo method; $n(x,y) = 5[1 - 0.4356(x^2/L_x^2 + y^2/L_y^2)]^{0.5}$, $T_1 = T_2 = T_3 = 0$ K, $T_4 = 1000$ K, $\kappa = 10$ m^{-1}, $L_x = L_y = 0.1$ m, $N_x = N_y = 20$, and $N_\theta = N_\varphi = 50$.

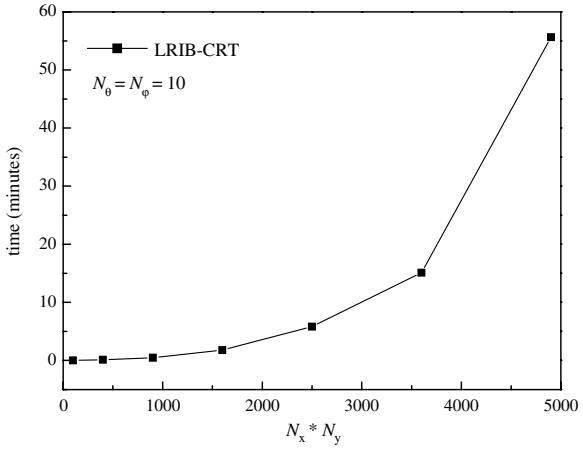

Fig. 6 Calculation times from LRIC-CRT for different numbers of spatial nodes; $n(x,y) = 1.1 + 0.6x/L_x + 0.2y/L_y$, $\kappa = 10$ m^{-1}, $L_x = L_y = 0.1$ m, and $N_\theta = N_\varphi = 10$.

$$\frac{I_m(s,\theta_i,\varphi_j)}{n^2(s)} = \frac{\sigma T_{m1}^4}{\pi}(1 - e^{-\kappa s_1}) + e^{-\kappa s_1}\frac{\sigma T_{m2}^4}{\pi}(1 - e^{-\kappa s_2}) + e^{-\kappa(s_1+s_2)}\frac{\sigma T_{m3}^4}{\pi}(1 - e^{-\kappa s_3}) + \cdots + e^{-\kappa(s_1+s_2+\cdots+s_{p-1})}\frac{\sigma T_{mp}^4}{\pi}(1 - e^{-\kappa s_p}) + e^{-\kappa(s_1+s_2+\cdots+s_{p-1}+s_p)}\frac{\sigma T_{bq}^4}{\pi} \tag{7}$$

When we trace back the ray from the position s and direction (θ_i, φ_j), the starting location of the ray is on one segment of the boundary q, where T_{bq} is the temperature of this boundary. In this process, the ray passes through p cells, mi $(i = 1, 2, \ldots, p)$ is the number of each cell, and s_i $(i = 1, 2, \ldots, p)$ is the length of the route in each cell.

Based on these analyses, the energy-balance equation can thus be transformed into the following discrete form:

$$T_i^4 = \sum_{m=1}^{N_x \times N_y} a_{im} T_m^4 + \sum_{k=1}^{2N_x+2N_y} c_{ik} T_{bk}^4 \qquad (i = 1, 2, \ldots, N_x \times N_y) \tag{8}$$

where a_{im} and c_{ik} are coefficients denoting the influences of T_m and T_{bk}, respectively. These coefficients can be determined using the ray-tracing process.

III. Numerical Results and Discussion

In this section, we compare the numerical results given by cell-RT and LRIC-CRT and discuss the calculation efficiency of the two methods. Also, we study the temperature field of the medium and discuss the influences on it. The cross-sectional area of the medium is 0.1×0.1 m^2.

A. Isothermal Condition of the Boundaries

Because an analytical solution of the temperature field for a two-dimensional GRIN medium is nonexistent, we will use a simple method to verify our calculation program. We assume that the four boundaries of the medium have the same temperature of 1 K, and so the temperature of the medium must be 1 K. However, the numerical results will cause a little difference.

Figure 4 shows the temperature map calculated by LRIC-CRT. The minimum value is 1.0000546 K at position (0.09875, 0.09875), and the maximum value is 1.0000825 K at position (0.04375, 0.04875). The temperature map calculated by cell-RT is not shown because it is very similar to Fig. 4. The minimum value found by cell-RT is 1.0000550 K, and the maximum value is 1.0000826 K. Both are located at the same position as seen in the LRIC-CRT results.

The results show that both LRIC-CRT and cell-RT can yield good results, and LRIC-CRT can obtain higher precision than can cell-RT.

B. Comparison of the Results with the Benchmark Solution

Liu [23] analyzed the radiative equilibrium temperature field of a medium with a special refractive-index distribution:

$$n(x,y) = 5[1 - 0.4356(x^2/L_x^2 + y^2/L_y^2)]^{0.5}$$

The results from the Monte Carlo method are presented as benchmark solutions. Table 1 and Fig. 5 give the results of this paper and the benchmark solutions in [23]. They show that the results of the cell-RT and LRIC-CRT methods fit the benchmark solutions well. For calculation with spatial node numbers $N_x = N_y = 20$, the maximum relative error from the benchmark solution is less than 2.5%. For calculation with $N_x = N_y = 60$, the maximum relative error from the benchmark solution is less than 0.8%. In these calculations, the directional node numbers are $N_\theta = N_\varphi = 50$.

Table 2 CPU time required by LRIC-CRT (CPU-Pentium D 3.4 GHz)[a]

N_x	N_y	CPU time by LRIC-CRT
10	10	1 s
20	20	7 s
30	30	29 s
40	40	1 min 40 s
50	50	5 min 50 s
60	60	15 min 6 s
70	70	55 min 37 s

[a] $n(x,y) = 1.1 + 0.6x/L_x + 0.2y/L_y$, $\kappa = 10$ m^{-1}, $L_x = L_y = 0.1$ m, and $N_\theta = N_\varphi = 10$.

Table 3 Comparison of the CPU time required by the cell-RT and LRIC-CRT (CPU–Pentium D 3.4 GHz)[a]

N_θ	N_φ	CPU time by LRIC-CRT	CPU time by cell-RT
10	10	1 min 48 s	1 min 32 s
20	20	3 min 59 s	2 min 47 s
30	30	7 min 32 s	4 min 51 s
40	40	12 min 29 s	7 min 50 s
50	50	18 min 52 s	11 min 32 s
60	60	26 min 40 s	16 min 11 s
70	70	35 min 51 s	21 min 36 s

[a] $n(x,y) = 1.1 + 0.6x/L_x + 0.2y/L_y$, $\kappa = 10$ m^{-1}, $L_x = L_y = 0.1$ m, and $N_x = N_y = 40$.

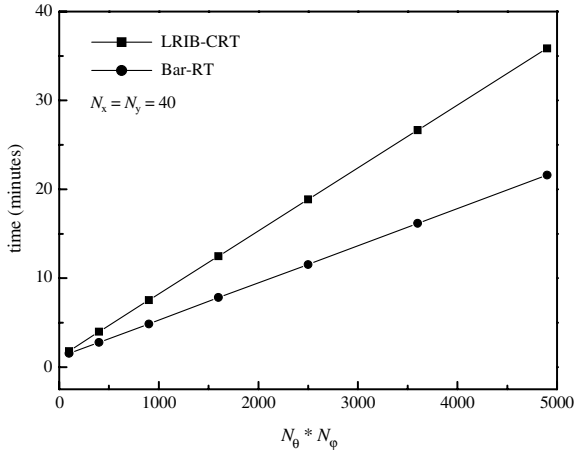

Fig. 7 Calculation times from LRIC-CRT and cell-RT for different numbers of directional nodes; $n(x,y) = 1.1 + 0.6x/L_x + 0.2y/L_y$, $\kappa = 10\ \mathrm{m}^{-1}$, $L_x = L_y = 0.1$ m, and $N_x = N_y = 40$.

Table 4 Temperature difference compared with the standard result; $N_x = N_y = 40$

N_θ	N_φ	ΔT, K Max	ΔT, K Min	δ%, max
		Cell-RT		
10	10	5.111	−5.565	2.038
20	20	7.982	−1.807	3.501
30	30	4.334	−2.052	1.884
40	40	6.395	−0.935	2.525
50	50	5.001	−0.880	2.014
60	60	6.237	−1.132	2.523
70	70	5.411	−0.869	2.154
		LRIC-CRT[a]		
10	10	3.685	−7.365	2.654
20	20	3.000	−1.767	1.213
30	30	1.223	−1.029	0.501
40	40	0.803	−0.817	0.319
50	50	1.133	−1.000	0.406
60	60	0.796	−0.495	0.261

[a] $n(x,y) = 1.1 + 0.6x/L_x + 0.2y/L_y$, $\kappa = 10\ \mathrm{m}^{-1}$, $L_x = L_y = 0.1$ m, $T_1 = 100$ K, $T_2 = 200$ K, $T_3 = 300$ K, and $T_4 = 400$ K.

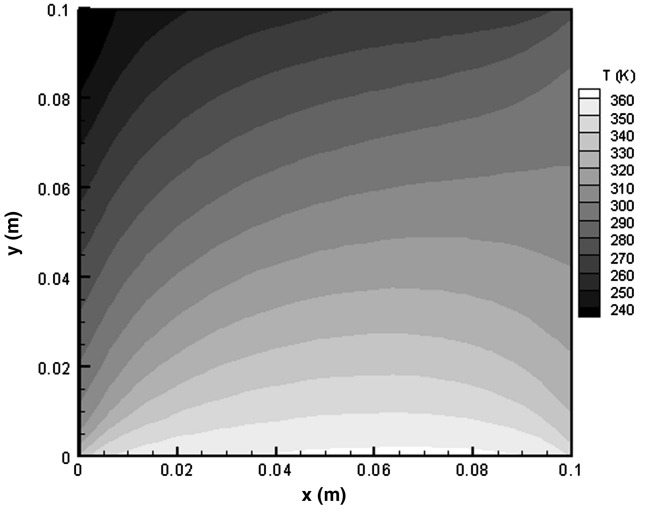

a) $N_x = N_y = 40$, $N_\theta = N_\varphi = 70$

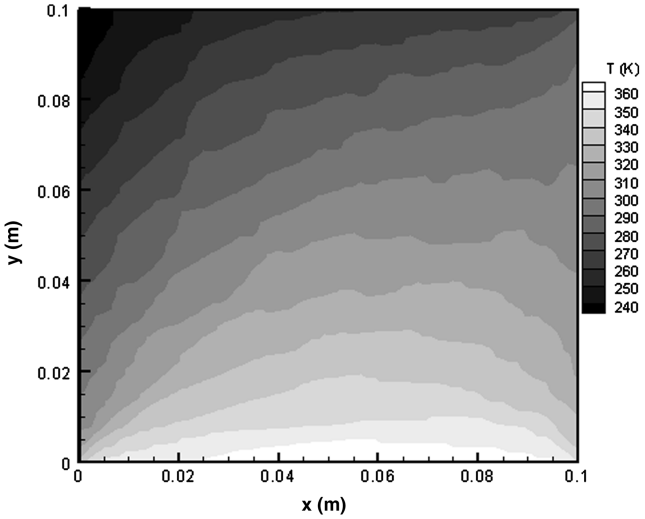

b) $N_x = N_y = 70$, $N_\theta = N_\varphi = 10$

Fig. 8 Temperature map of medium using LRIC-CRT; $n(x,y) = 1.1 + 0.6x/L_x + 0.2y/L_y$, $\kappa = 10\ \mathrm{m}^{-1}$, $L_x = L_y = 0.1$ m, $T_1 = 100$ K, $T_2 = 200$ K, $T_3 = 300$ K, and $T_4 = 400$ K.

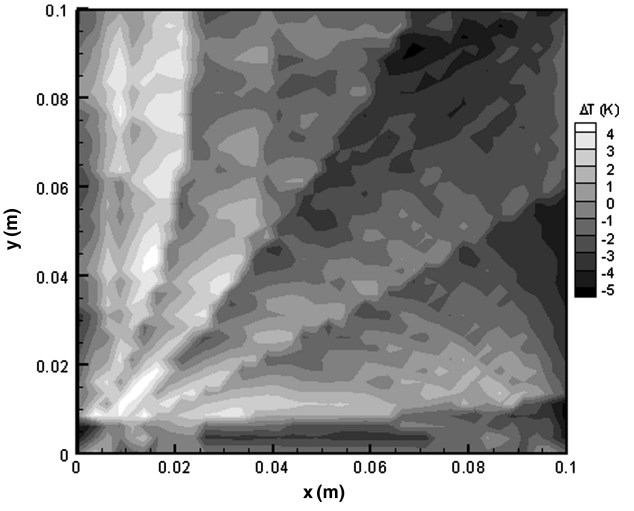

a) ΔT

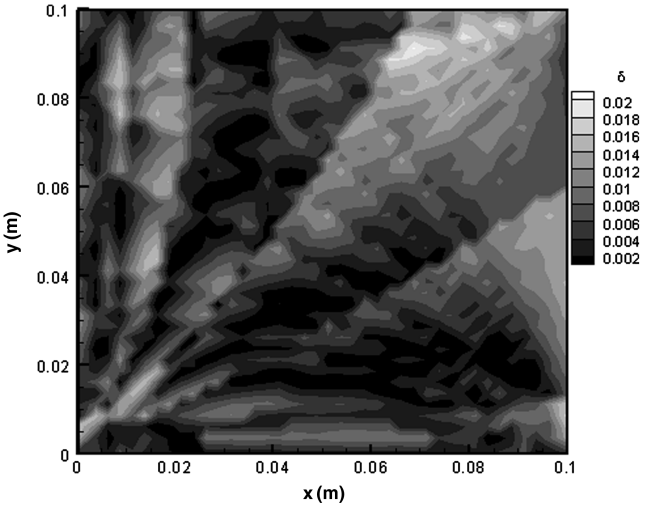

b) δ

Fig. 9 Map of temperature difference ΔT and relative error δ of the results from LRIC-CRT ($N_x = N_y = 40$ and $N_\theta = N_\varphi = 10$) compared with the standard results; $n(x,y) = 1.1 + 0.6x/L_x + 0.2y/L_y$, $\kappa = 10\ \mathrm{m}^{-1}$, $L_x = L_y = 0.1$ m, $T_1 = 100$ K, $T_2 = 200$ K, $T_3 = 300$ K, and $T_4 = 400$ K.

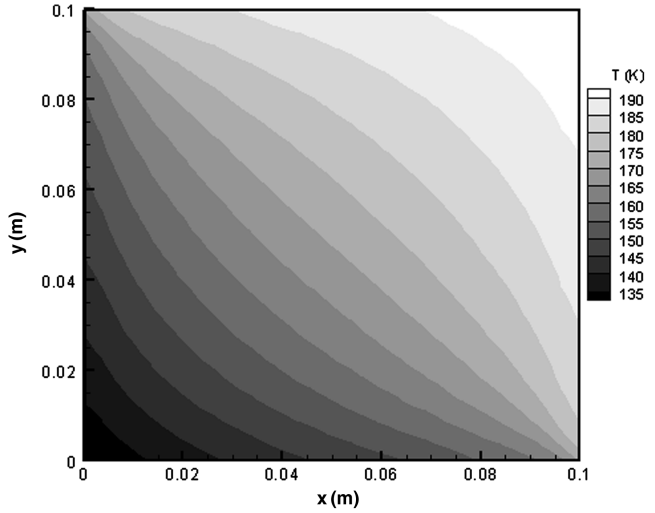

Fig. 10 Temperature map of medium with constant-refractive-index distribution from LRIC-CRT; $T_1 = T_4 = 100$ K, $T_2 = T_3 = 200$ K, $\kappa = 10$ m^{-1}, $L_x = L_y = 0.1$ m, $N_x = N_y = 40$, and $N_\theta = N_\varphi = 100$.

In the early 1990s, Siegel and Spuckler [20] expressed the idea that increasing the number of sublayers could approach the radiative behavior of a medium with a continuously varying refractive index. The results in Table 1 show that Siegel and Spuckler's idea can be employed to solve multidimensional radiative heat transfer problems. These two approximate models can easily deal with arbitrary refractive-index distributions.

C. Comparison of Calculation Time

Calculation time will change with the number of spatial nodes N_x and N_y. Table 2 shows the CPU time used by LRIC-CRT. The number of directional nodes N_θ and N_φ are each 10. The results show that the calculation time will increase greatly with an increase of N_x and N_y. When the medium is discretized into 10×10 cells, the calculation time is only 1 s. When the medium has 70×70 cells, however, the calculation time goes up to about 1 h. We also plot the calculation time in Fig. 6, which clearly displays the time increase with increasing number of spatial nodes. It shows that we cannot adopt large values of N_x and N_y. However, if we use values such as 40×40 or 50×50, this will be enough to treat a two-dimensional problem.

Calculation time also will change with the number of directional nodes N_θ and N_φ. Table 3 shows the CPU time used by the LRIC-CRT method and the cell-RT method, where N_x and N_y are both

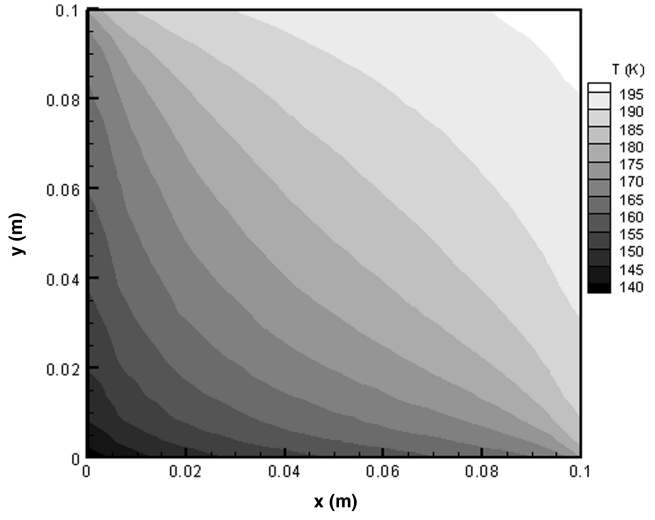

a) $n(x,y) = 1.1 + 0.6x / L_x + 0.6y / L_y$

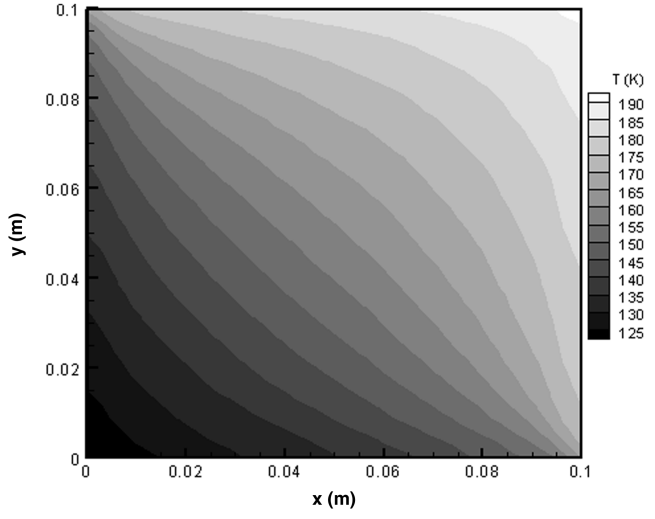

b) $n(x,y) = 2.3 - 0.6x / L_x - 0.6y / L_y$

Fig. 11 Temperature map of medium with linear refractive-index distribution from LRIC-CRT; $T_1 = T_4 = 100$ K, $T_2 = T_3 = 200$ K, $\kappa = 10$ m^{-1}, $L_x = L_y = 0.1$ m, $N_x = N_y = 40$, and $N_\theta = N_\varphi = 100$.

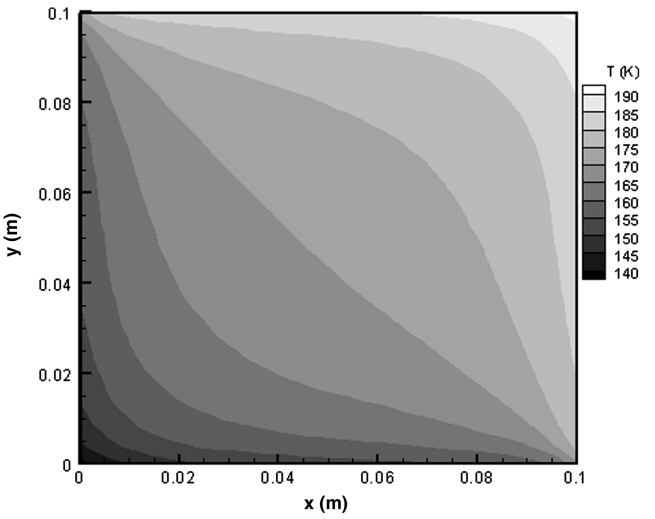

a) $n(x,y) = 1.1 + 0.6\sin(\pi x / L_x) + 0.6\sin(\pi y / L_y)$

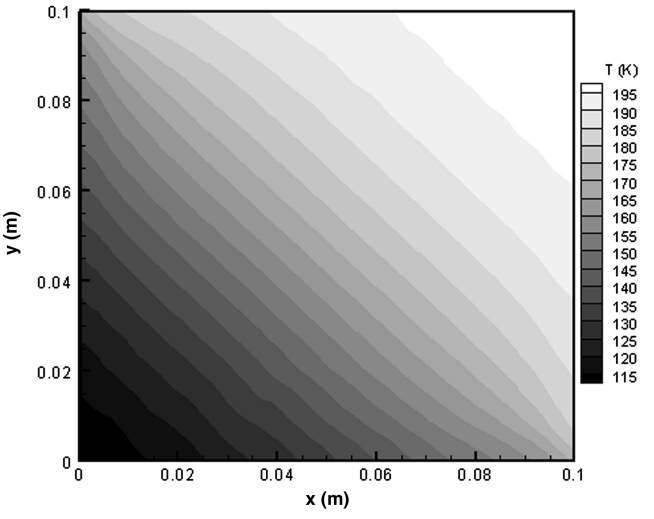

b) $n(x,y) = 2.3 - 0.6\sin(\pi x / L_x) - 0.6\sin(\pi y / L_y)$

Fig. 12 Temperature map of medium with nonlinear refractive-index distribution from LRIC-CRT; $T_1 = T_4 = 100$ K, $T_2 = T_3 = 200$ K, $\kappa = 10$ m^{-1}, $L_x = L_y = 0.1$ m, $N_x = N_y = 40$, and $N_\theta = N_\varphi = 100$.

Table 5 Maximum temperature and minimum temperature in a medium for different refractive-index distributions from LRIC-CRT[a]

$n(x, y)$	T_{max}, K	T_{min}, K
$4.1 - 1.5x/L_x - 1.5y/L_y$	189.8	115.5
$2.3 - 0.6x/L_x - 0.6y/L_y$	191.4	120.9
const	193.9	130.1
$1.1 + 0.6x/L_x + 0.6y/L_y$	196.4	137.6
$1.1 + 1.5x/L_x + 1.5y/L_y$	197.5	141.7

[a]$T_1 = T_4 = 100$ K, $T_2 = T_3 = 200$ K, $\kappa = 10$ m^{-1}, $L_x = L_y =$ 0.1 m, $N_x = N_y = 40$, and $N_\theta = N_\varphi = 100$.

equal to 40. This table shows that the calculation time for LRIC-CRT is larger than that of cell-RT. The calculation times of these two methods increase linearly with an increase in the number of spatial nodes (see Fig. 7).

D. Comparison of Temperature-Field Results

Figure 8a shows the temperature field calculated by LRIC-CRT ($N_x = N_y = 40$ and $N_\theta = N_\varphi = 70$). We use this result as a standard to compare with other results. We have two reasons for this selection. First, the results from LRIC-CRT have a higher precision than those from cell-RT. Second, the number of spatial and directional nodes is large enough for the calculation to be accurate. Figure 8b shows the temperature field calculated by LRIC-CRT for $N_x = N_y = 70$ and $N_\theta = N_\varphi = 10$. It reveals that the isothermal lines have rough edges, which is due to N_θ and N_φ being too small. Therefore, we discuss the influence of N_θ and N_φ in the following.

Table 4 displays the temperature difference ΔT and relative error δ for different numbers of directional nodes. The definitions of ΔT and δ are

$$\Delta T = T_{standard} - T \tag{9}$$

$$\delta = \frac{|T_{standard} - T|}{T_{standard}} \tag{10}$$

Comparing the results of cell-RT with the standard results shows that the temperature difference between them does not decrease significantly with increasing numbers of directional nodes. The maximum value of ΔT is about 5–6 K, and the maximum value of δ is about 2–2.5%. Comparing the results of LRIC-CRT to the standard results shows that the temperature differences between them obviously decrease as the number of directional nodes increases.

Figure 9 shows the temperature difference between the results of LRIC-CRT ($N_x = N_y = 40$ and $N_\theta = N_\varphi = 10$) and the standard results, as well as the relative error. In most regions, the results are almost the same.

E. Influence of the Refractive Index Distribution on the Temperature Field

Figures 10–12 show the temperature maps of the constant-refractive-index medium, the linear refractive-index medium and the nonlinear refractive-index medium from LRIC-CRT. In the calculations, boundaries 1 and 4 have a temperature of 100 K, and boundaries 2 and 3 have a temperature of 200 K. The absorption coefficient κ is 10 m^{-1} and $N_x = N_y = 40$ and $N_\theta = N_\varphi = 100$.

In the constant-refractive-index medium, the maximum temperature T_{max} is 193.9 K and the minimum temperature T_{min} is 130.1 K (see Fig. 10 and Table 5). The difference between them is 63.8 K. The medium with

$$n(x, y) = 1.1 + 0.6x/L_x + 0.6y/L_y$$

has higher temperatures than those of the constant index medium, and the medium with

$$n(x, y) = 2.3 - 0.6x/L_x - 0.6y/L_y$$

has lower temperatures than those of the constant index medium (see Fig. 11 and Table 5). In the medium with

$$n(x, y) = 1.1 + 0.6\sin(\pi x/L_x) + 0.6\sin(\pi y/L_y)$$

the difference between T_{max} and T_{min} is 53.4 K, which is smaller than that of the constant index medium. In the medium with

$$n(x, y) = 2.3 - 0.6\sin(\pi x/L_x) - 0.6\sin(\pi y/L_y)$$

the difference between T_{max} and T_{min} is 88.0 K, which is larger than that of the constant index medium (see Fig. 12 and Table 6).

In the medium with

$$n(x, y) = 1.1 + 0.6x/L_x + 0.6y/L_y$$

the region near the high-temperature boundaries (boundaries 2 and 3) is optically denser than the rest of the medium, and the region near the low-temperature boundaries (boundaries 1 and 4) is optically thinner. When a ray propagates from the optically denser region to the optically thinner region, total reflection will occur. This means that the high-temperature boundary influence on the temperature field is enhanced. Therefore, the temperatures are higher than for the medium of constant refractive index. For the same reason, when the medium has a refractive index

$$n(x, y) = 2.3 - 0.6x/L_x - 0.6y/L_y$$

the low-temperature boundary influence on the temperature field is enhanced, and the temperatures are lower than for the constant index medium (see Fig. 11b and Table 5).

In the medium with

$$n(x, y) = 1.1 + 0.6\sin(\pi x/L_x) + 0.6\sin(\pi y/L_y)$$

the region near the four boundaries is optically thinner, and the central area is optically denser. Total internal reflection can make the temperature field flatter than for the constant-refractive-index medium (see Table 6). In the medium with

$$n(x, y) = 2.3 - 0.6\sin(\pi x/L_x) - 0.6\sin(\pi y/L_y)$$

the region near the four boundaries is optically denser, and the central area is optically thinner. Total internal reflection enhances the boundary influence on the nearby region. As a result, the value of $T_{max} - T_{min}$ is greater than for the constant-refractive-index medium (see Table 6).

Table 6 Difference between maximum temperature and minimum temperature in a medium for different refractive-index distributions from LRIC-CRT[a]

$n(x, y)$	T_{max}, K	T_{min}, K	$T_{max} - T_{min}$, K
$1.1 + 1.5\sin(\pi x/L_x) + 1.5\sin(\pi y/L_y)$	190.1	140.9	49.2
$1.1 + 0.6\sin(\pi x/L_x) + 0.6\sin(\pi y/L_y)$	191.3	137.9	53.4
const	193.9	130.1	63.8
$2.3 - 0.6\sin(\pi x/L_x) - 0.6\sin(\pi y/L_y)$	198.5	110.5	88.0
$4.1 - 1.5\sin(\pi x/L_x) - 1.5\sin(\pi y/L_y)$	199.4	104.3	95.1

[a]$T_1 = T_4 = 100$ K, $T_2 = T_3 = 200$ K, $\kappa = 10$ m^{-1}, $L_x = L_y = 0.1$ m, $N_x = N_y = 40$, and $N_\theta = N_\varphi = 100$.

These are the mirage effects of a GRIN medium and they will be more obvious when the gradient of the refractive index is increased (see Tables 5 and 6).

IV. Conclusions

This paper presents two methods for the study of radiative heat transfer in a two-dimensional graded-index semitransparent medium. One is a combination of the cell model and the ray-tracing technique (cell-RT), and the other is a combination of the linear refractive-index cell model and the discrete curved-ray-tracing technique (LRIC-CRT). When the ray-tracing process is replaced by a Monte Carlo ray-tracing process, these two methods can be applied to deal with scattering media.

We compared the results and the calculation efficiency of these two methods. For the cases considered, the maximum difference in temperature between these two methods is about 2%. The calculation time will increase sharply with an increase in the number of spatial nodes and will increase linearly with an increase in the number of directional nodes.

The results show that with the mirage effect of a GRIN medium, the refractive-index distribution has an important influence on the temperature field. For various types of graded indices, a medium has higher or lower temperatures than those of a medium with a constant refractive index, and a GRIN medium also has a flatter temperature field or sharper temperature field than that of a constant-refractive-index medium.

Acknowledgments

This work was supported by the National Science Foundation of China (no. 50606003) and the Aeronautic Science Foundation (no. 2007ZA51006) of China.

References

[1] Qiao, Y. T., *Gradient Index Optics*, Beijing: Science Press, Marrickville, NSW, Australia, 1990.

[2] Ben Abdallah, P., and Le Dez, V., "Thermal Emission of a Semi-Transparent Slab with Variable Spatial Refractive Index," *Journal of Quantitative Spectroscopy and Radiative Transfer*, Vol. 67, No. 3, 2000, pp. 185–198. doi:10.1016/S0022-4073(99)00205-8

[3] Ben Abdallah, P., and Le Dez, V., "Temperature Field Inside an Absorbing-Emitting Semitransparent Slab at Radiative Equilibrium with Variable Spatial Refractive Index," *Journal of Quantitative Spectroscopy and Radiative Transfer*, Vol. 65, No. 4, 2000, pp. 595–608. doi:10.1016/S0022-4073(99)00111-9

[4] Ben Abdallah, P., and Le Dez, V., "Radiative Flux Field Inside an Absorbing-Emitting Semi-Transparent Slab with Variable Spatial Refractive Index at Radiative Conductive Coupling," *Journal of Quantitative Spectroscopy and Radiative Transfer*, Vol. 67, No. 2, 2000, pp. 125–137. doi:10.1016/S0022-4073(99)00200-9

[5] Ben Abdallah, P., and Le Dez, V., "Thermal Emission of a Two Dimensional Rectangular Cavity with Spatial Affine Refractive Index," *Journal of Quantitative Spectroscopy and Radiative Transfer*, Vol. 66, No. 6, 2000, pp. 555–569. doi:10.1016/S0022-4073(99)00185-5

[6] Huang, Y., Tan, H. P., and Xia, X. L., "Apparent Emitting Characteristics of Semi-Transparent Isothermal Medium Layer with Graded Index," *Journal of Infrared and Millimeter Waves*, Vol. 20, No. 5, 2001, pp. 348–352 (in Chinese).

[7] Huang, Y., Xia, X. L., and Tan, H. P., "Temperature Fields Inside an Absorbing-Emitting Semi-Transparent Slab at Radiative Equilibrium with Linear Graded Index and Gray Walls," *Journal of Quantitative Spectroscopy and Radiative Transfer*, Vol. 74, No. 2, 2002, pp. 249–261. doi:10.1016/S0022-4073(01)00238-2

[8] Lemonnier, D., and Le Dez, V., "Discrete Ordinates Solution of Radiative Transfer Across a Slab with Variable Refractive Index," *Journal of Quantitative Spectroscopy and Radiative Transfer*, Vol. 73, No. 2–5, 2002, pp. 195–204. doi:10.1016/S0022-4073(01)00222-9

[9] Yi, H. L., Tan, H. P., Luo, J. F., and Dong, S. K., "Effects of Graded Refractive Index on Steady and Transient Heat Transfer Inside a Scattering Semitransparent Slab," *Journal of Quantitative Spectroscopy and Radiative Transfer*, Vol. 96, No. 3–4, 2005, pp. 363–381. doi:10.1016/j.jqsrt.2004.12.034

[10] Tan, H. P., Yi, H. L., Luo, J. F., and Zhang, H. C., "Transient Coupled Heat Transfer Inside a Scattering Medium with Graded Refractive Index," *Journal of Thermophysics and Heat Transfer*, Vol. 20, No. 3, 2006, pp. 583–594. doi:10.2514/1.15824

[11] Huang, Y., Xia, X. L., and Tan, H. P., "Comparison of Two Methods for Solving Radiative Heat Transfer in a Gradient Index Semitransparent Slab," *Numerical Heat Transfer, Part B, Fundamentals*, Vol. 44, No. 1, 2003, pp. 83–99. doi:10.1080/713836336

[12] Liu, L. H., "Finite Volume Method for Radiation Heat Transfer in Graded Index Medium," *Journal of Thermophysics and Heat Transfer*, Vol. 20, No. 1, 2006, pp. 59–66. doi:10.2514/1.12459

[13] Liu, L. H., "Meshless Method for Radiation Heat Transfer in Graded Index Medium," *International Journal of Heat and Mass Transfer*, Vol. 49, No. 1–2, 2006, pp. 219–229. doi:10.1016/j.ijheatmasstransfer.2005.07.013

[14] Krishna, N. A., and Mishra, S. C., "Discrete Transfer Method Applied to Radiative Transfer in a Variable Refractive Index Semitransparent Medium," *Journal of Quantitative Spectroscopy and Radiative Transfer*, Vol. 102, No. 3, 2006, pp. 432–440. doi:10.1016/j.jqsrt.2006.02.024

[15] Sun, Y. S., and Li, B. W., "Chebyshev Collocation Spectral Method for One Dimensional Radiative Heat Transfer in Graded Index Media," *International Journal of Thermal Sciences*, Vol. 48, No. 4, 2009, pp. 691–698. doi:10.1016/j.ijthermalsci.2008.07.003

[16] Liu, L. H., Zhang, L., and Tan, H. P., "Finite Element Method for Radiation Heat Transfer in Multi-Dimensional Graded Index Medium," *Journal of Quantitative Spectroscopy and Radiative Transfer*, Vol. 97, No. 3, 2006, pp. 436–445. doi:10.1016/j.jqsrt.2005.05.067

[17] Liu, L. H., "Least-Squares Finite Element Method for Radiation Heat Transfer in Graded Index Medium," *Journal of Quantitative Spectroscopy and Radiative Transfer*, Vol. 103, No. 3, 2007, pp. 536–544. doi:10.1016/j.jqsrt.2006.07.005

[18] Liu, L. H., and Liu, L. J., "Discontinuous Finite Element Method for Radiative Heat Transfer in Semitransparent Graded Index Medium," *Journal of Quantitative Spectroscopy and Radiative Transfer*, Vol. 105, No. 3, 2007, pp. 377–387. doi:10.1016/j.jqsrt.2006.11.017

[19] Zhao, J. M., and Liu, L. H., "Solution of Radiative Heat Transfer in Graded Index Media by Least Square Spectral Element Method," *International Journal of Heat and Mass Transfer*, Vol. 50, No. 13–14, 2007, pp. 2634–2642. doi:10.1016/j.ijheatmasstransfer.2006.11.032

[20] Siegel, R., and Spuckler, C. M., "Variable Refractive Index Effects on Radiation in Semitransparent Scattering Multilayered Regions," *Journal of Thermophysics and Heat Transfer*, Vol. 7, No. 4, 1993, pp. 624–630. doi:10.2514/3.470

[21] Huang, Y., and Liang, X. G., "Approximate Thermal Emission Models of a Two-Dimensional Graded Index Semitransparent Medium," *Journal of Thermophysics and Heat Transfer*, Vol. 20, No. 1, 2006, pp. 52–58. doi:10.2514/1.10360

[22] Huang, Y., Dong, S. J., Yang, M., and Wang, J., "Thermal Emission Characteristics of a Graded Index Semitransparent Medium," *Journal of Quantitative Spectroscopy and Radiative Transfer*, Vol. 109, No. 12–13, 2008, pp. 2141–2150. doi:10.1016/j.jqsrt.2008.04.002

[23] Liu, L. H., "Benchmark Numerical Solutions for Radiative Heat Transfer in Two-Dimensional Medium with Graded Index Distribution," *Journal of Quantitative Spectroscopy and Radiative Transfer*, Vol. 102, No. 2, 2006, pp. 293–303. doi:10.1016/j.jqsrt.2006.02.014